Biology of Reproduction, 2018, 98(6), 856–869
doi:10.1093/biolre/ioy060
Research Article
Advance Access Publication Date: 13 March 2018

OXFORD

Research Article

Uterine function in the mouse requires speckle-type poz protein†

Lan Hai[1], Maria M. Szwarc[1], Bin He[1], David M. Lonard[1], Ramakrishna Kommagani[2], Francesco J. DeMayo[3] and John P. Lydon[1,*]

[1]Department of Molecular and Cellular Biology, Baylor College of Medicine, Houston, Texas, USA; [2]Department of Obstetrics and Gynecology, Washington University School of Medicine, St. Louis, Missouri, USA and [3]Reproductive and Developmental Biology Laboratory, National Institute of Environmental Health Sciences, Research Triangle Park, North Carolina, USA

*__Correspondence:__ Department of Molecular and Cellular Biology Baylor College of Medicine, One Baylor Plaza, Houston, TX 77030, USA. Tel: +(713) 798-3534; Fax: +(713) 790-1275; E-mail: jlydon@bcm.edu

†__Grant Support:__ This research was supported in part by a Cancer Prevention Research Institute of Texas pre-doctoral fellowship grant (CPRIT: RP101499 (to MMS)); National Institutes of Health (NIH)/National Institute of Child Health and Human Development (NICHD) grant (U01: HD-076596 (to DML)); a NIH/NCI R01: CA-211861 to BH; a NIH/NICHD K99 HD080742 to RK; and a NIH/NICHD: R01: HD-042311 grant (to JPL).

Received 9 January 2018; Revised 7 February 2018; Accepted 6 March 2018

Abstract

Speckle-type poz protein (SPOP) is an E3-ubiquitin ligase adaptor for turnover of a diverse number of proteins involved in key cellular processes such as chromatin remodeling, transcriptional regulation, and cell signaling. Genomic analysis revealed that *SPOP* somatic mutations are found in a subset of endometrial cancers, suggesting that these mutations act as oncogenic drivers of this gynecologic malignancy. These studies also raise the question as to the role of wild-type SPOP in normal uterine function. To address this question, we generated a mouse model (*Spop*$^{d/d}$) in which SPOP is ablated in uterine cells that express the PGR. Fertility studies demonstrated that SPOP is required for embryo implantation and for endometrial decidualization. Molecular analysis revealed that expression levels of the PGR at the protein and transcript level are significantly reduced in the *Spop*$^{d/d}$ uterus. While this result was unexpected, this finding explains in part the dysfunctional phenotype of the *Spop*$^{d/d}$ uterus. Moderate increased levels of the ESR1, GATA2, and SRC2 were detected in the *Spop*$^{d/d}$ uterus, suggesting that SPOP is required to maintain the proteome for normal uterine function. With age, the *Spop*$^{d/d}$ endometrium exhibits large glandular cysts with foci of epithelial proliferation, further supporting a role for SPOP in maintaining a healthy uterus. Collectively, studies on the *Spop*$^{d/d}$ mouse support an important role for SPOP in normal uterine function and suggest that this mouse model may prove useful to study the role of SPOP-loss-of-function mutations in the etiopathogenesis of endometrial cancer.

Summary Sentence

SPOP is required for embryo implantation, endometrial decidualization, and uterine health in the mouse

Key words: mouse, speckle-type poz protein, progesterone receptor, estrogen receptor, embryo implantation, decidualization.

Introduction

Efforts to improve diagnosis and treatment of uterine dysfunction are stymied by an incomplete understanding of the key endometrial molecular signals that are required for early establishment of the maternofetal interface. Recent whole exome sequencing has revealed that speckle-type poz (pox virus and zinc finger) protein (SPOP; also known as PCIF1 [1]) is frequently mutated in human endometrial cancers [2–5]. This observation suggests that *SPOP* mutations may act as oncogenic drivers of this gynecological malignancy and raises the question: Is wild-type SPOP required for normal uterine biology? Acting as a 42 kDa adaptor protein for the cullin3 (CUL3)-based E3 ubiquitin ligase complex, SPOP is composed of a N-terminal MATH domain, which selectively recruits substrates for ubiquitination and subsequent proteasomal degradation (reviewed in [6, 7]). To date, all human endometrial cancer-associated SPOP mutations have been mapped to the MATH substrate-recognition cleft [7]; therefore, such mutations are predicted to block normal substrate recruitment for proteasomal turnover. Toward the C-terminus, the bric-a-brac/tramtrack/broad (BTB) domain of SPOP is required for interaction with the CUL3 scaffold protein [6, 7], which then targets substrates for ubiquitin-mediated degradation by the 26S proteasome.

Underscoring its evolutionary conserved and pleiotropic role in proteome homeostasis, SPOP is associated with the ubiquitination and degradation of a rapidly expanding list of diverse substrates involved in a broad spectrum of physiological processes. Some of these substrates include Daxx, the death-associated protein; Puckered (Puc), a signaling phosphatase; MacroH2A, a core histone variant; Gli (glioma associated oncogene), a transcriptional regulator; CHOP (C/EBP homologous protein), a transcription factor; CDC20 (cell division cycle 20), a cell cycle regulator; ERG (ETS-related gene), an ETS transcription factor family member; AR (androgen receptor), a nuclear transcription factor; coactivators: steroid receptor coactivator-3 (SRC-3) and tripartite motif containing 24 (TRIM 24), and more recently c-MYC [8–20]. Although wild-type SPOP is considered a tumor suppressor in a number of human cancers (reviewed in [7]), high expression levels of wild-type SPOP have been shown to act as a tumor promoter in other target tissues such as the kidney [21–24]. These paradoxical findings may be explained in part by the cell-type specific make-up of a given SPOP substrate population, which may constitute either a majority of tumor suppressors or tumor promoters depending on cellular context [7].

Although there is compelling evidence that mutations of SPOP may drive endometrial cancer, the in vivo role of wild-type SPOP in normal uterine function is not known. To address this issue, we recently applied conditional genetic technology in the mouse to selectively abrogate SPOP expression in uterine cells that express the PGR. Our data strongly support an important role for SPOP in normal uterine function in the mouse by regulating the homeostasis of key signaling cues required for embryo implantation and endometrial decidualization.

Materials and methods

Generation of a *Spop* conditional knockout mouse

As described previously [13, 25], C57BL/6 mice carrying the $Spop^{tm1a(KOMP)Wtsi}$ allele were obtained from the international knockout mouse phenotyping (KOMP) consortium (www.knockoutmouse.org). Termed a knockout first allele, the engineered $Spop^{tm1a(KOMP)Wtsi}$ allele consists of a targeted insertion into the third intron of the murine *Spop* gene. In the 5′ to 3′ direction, the insertion cassette is composed of an *FRT* site followed by the *LacZ* gene and a *loxP* site. The first *loxP* site is followed by a *neomycin resistance* (neo^r) gene under the control of the human *beta-actin* promoter; the antibiotic resistance gene also contains a strong SV40 polyA termination signal. A second *FRT* site and *loxP* site follow the neo^r gene, while a third *loxP* site is inserted downstream of exon 5 of the *Spop* gene. A "conditional ready" *Spop* allele, in which exons 4 and 5 are flanked by *loxP* sites (floxed), was generated by crossing $Spop^{tm1a(KOMP)Wtsi}$ mice with C57BL6 mice carrying the flip recombinase gene (encoding flippase) targeted to the *ROSA* locus [26]. Progeny carrying a *Spop* conditional allele ($Spop^{f/f}$) was crossed with our Pgr^{cre} mice (*Pgr* < *tm2(cre)Lyd* > (C57BL6)) to selectively abrogate SPOP expression in cells expressing the PGR [27]. The PCR primer sequences used to genotype the $Spop^{tm1a(KOMP)Wtsi}$ allele are as follows: forward-primer 5′-GGGATCTCATGCTGGAGTTCTTC-3′; and reverse-primer 5′-GAGCGTTCACATCCCTTACATCTC-3′, which generates a 659-bp amplicon (PCR-1; Figure 1A and B). The PCR primer sequences to genotype the $Spop^{f/f}$ allele are as follows: forward-primer 5′-GCAGAAGCAGGCAGATCTTT-3′ and reverse-primer 5′-GCCCTTAGTTTTTCATGATGG-3′, which generates a 179-bp and 397-bp amplicon (PCR-2; Figure 1A and B) for the wild-type and floxed *Spop* allele respectively. For brevity, resultant Pgr^{cre}:$Spop^{f/f}$ bigenic mice are termed $Spop^{d/d}$. For studies described herein, Pgr^{cre} monogenics served as controls for $Spop^{d/d}$ mice. When possible, control and $Spop^{d/d}$ mice were euthanized at the same stage of their cycles for histological and molecular studies described herein.

Animal husbandry and housing was undertaken in an AAALAC accredited *vivarium* at Baylor College of Medicine. In temperature controlled mouse rooms (22 ± 2°C) on a 6 am–7 pm light cycle, mice were fed irradiated Tekland global soy protein-free extruded rodent diet (Harlan Laboratories, Inc., Indianapolis, IN) and fresh water ad libitum. Mouse experiments were conducted in strict accordance with the guidelines described in the Guide for the Care and Use of Laboratory Animals ("The Guide" (Eighth Edition 2011)) published by the National Research Council of the National Academies, Washington, D.C. (www.nap.edu). Animal protocols used in these studies were prospectively approved by the Institutional Animal Care and Use Committee at Baylor College of Medicine.

Fertility trials, timed pregnancies, and superovulation

For breeding trials, sexually mature control and $Spop^{d/d}$ females were housed with proven stud/breeder C57BL/6 males. Over a 6-month breeding period, the date of pup delivery, the number of litters, and the number of pups per litter were recorded for each female. For timed pregnancy studies, females were housed with fertility-proven C57BL/6 males overnight. The detection of a copulatory (or vaginal) plug the following morning was designated as day 1 of pregnancy (1 dpc); pregnant females were individually housed. To locate incipient implantation sites in uterine horns of 5-dpc pregnant dams, Chicago sky blue dye (1%; 100 μl PBS/mouse) was injected into one of the two lateral tail veins before mice were euthanized 2 min later.

To induce superovulation, 21-day old female mice were intraperitoneally (IP) injected with pregnant mare serum gonadotropin (PMSG; Sigma-Aldrich, St. Louis, MO (5 international units (IU)/100 μl of sterile 0.9% saline)). Forty-eight hours later, mice received an IP injection of human chorionic gonadotropin (hCG; Sigma-Aldrich (5 IU/100 μl of sterile 0.9% saline)). Sixteen hours post-hCG injection, oocytes were collected from oviducts and counted using a dissecting microscope as previously described

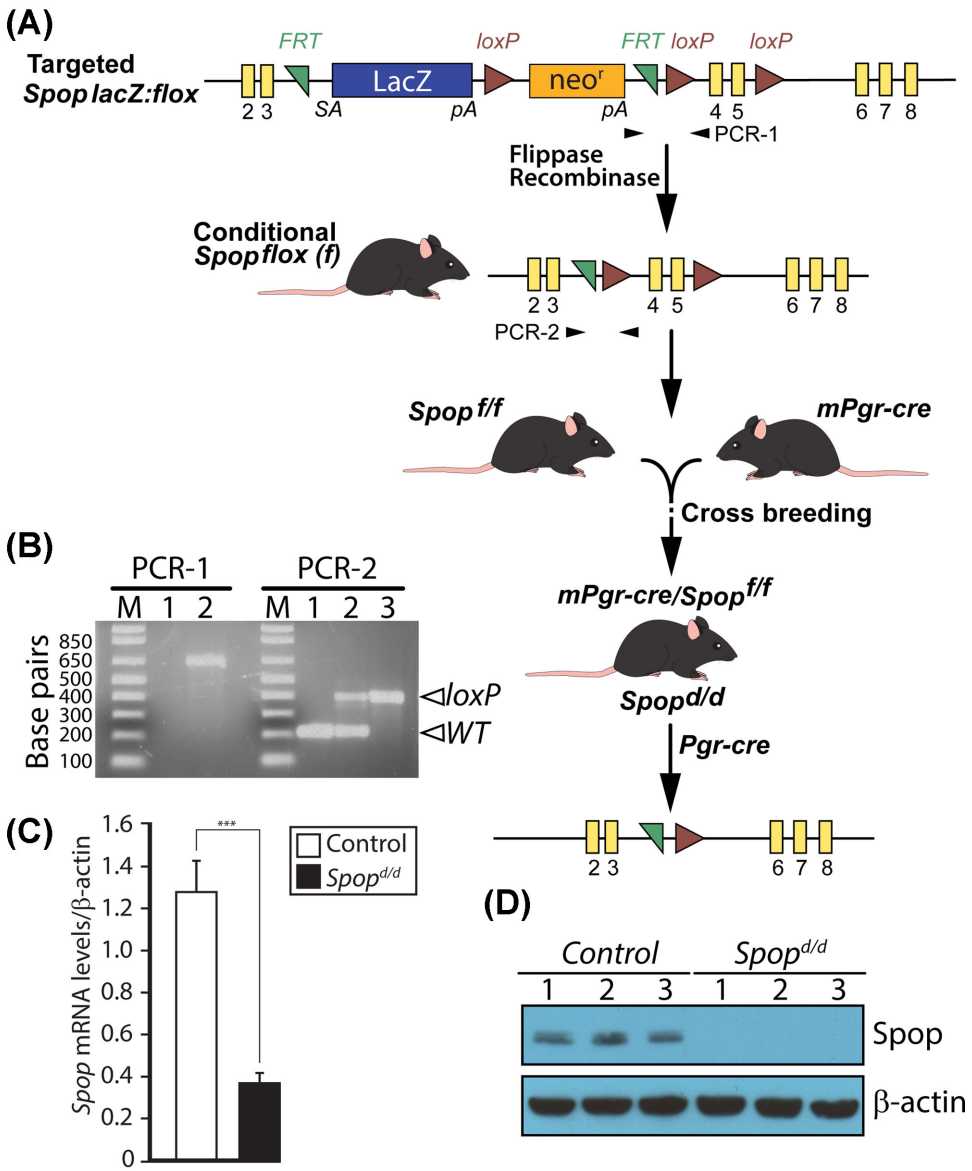

Figure 1. Generation of the *Spop*$^{d/d}$ mouse. (A) Obtained from KOMP [13], mice carrying the *Spop lacZ: flox* allele were crossed with ROSA *flippase* mice to generate mice harboring the conditional *Spop* floxed allele (*Spop*$^{f/f}$) in which exons 4 and 5 are flanked by *loxP* sites. The *Spop*$^{f/f}$ and *mPgr-cre* mouse (both C57BL6) were crossed to generate the bigenic *Spop*$^{d/d}$ mouse. Driven by the *Pgr* promoter, the cre recombinase excises exons 4 and 5 of the *Spop* gene in the *Spop*$^{d/d}$ mouse; exons 4 and 5 encode the essential MATH domain of SPOP [13]. (B) Typical PCR results are shown for genotyping mice carrying the targeted *Spop lacZ: flox* allele and the *Spop*$^{f/f}$ allele using the PCR-1 and PCR-2 reaction primers respectively. For the PCR-1 reaction, lanes 1 and 2 represent genotype results using tail tip genomic DNA from control mice and mice heterozygous for the *Spop lacZ: flox* allele, respectively; the positive PCR amplicon is 659 bp. For the PCR-2 reaction, lanes 1, 2, and 3 denote control, *Spop*$^{f/+}$ (heterozygous for the *Spop* floxed allele) and *Spop*$^{f/f}$ (homozygous for *Spop* floxed allele) respectively; PCR-positive amplicon is 179 bp for WT allele and 397 bp for *Spop* floxed allele. Primer sequences for PCR-1 and -2 are listed in Materials and methods section. (C) Real-time PCR analysis clearly demonstrates a significant reduction in *Spop* transcript levels in the uterus of *Spop*$^{d/d}$ mice (n = 9) as compared to controls (n = 6). (D) Western analysis of protein isolated from control and *Spop*$^{d/d}$ uteri confirms that SPOP protein is not detected in the *Spop*$^{d/d}$ uterus; each lane represents a protein sample pooled from four individual adult mice per genotype (β-actin serves as a loading control).

[28]. Ovaries were fixed in 4% paraformaldehyde (PFA) for histological analysis. To assess ovarian cyclicity, the estrous cycle was monitored over 3–4 weeks by examining the cytology of daily vaginal lavages on slides stained with 10% crystal violet (Sigma-Aldrich) [29].

To measure circulating serum levels of E2 and P4, blood was collected from the orbital sinus of anesthetized 5-dpc *Spop*$^{d/d}$ and control mice. After blood clotting at room temperature for 90 min in BD microtainer tubes (Fisher Scientific Inc.), serum was isolated through the microtainer tubes' serum separator; serum was stored at –80°C until hormone measurement. Serum levels of E2 and P4 were measured by the Ligand Assay and Analysis Core of the Center for Research in Reproduction at the University of Virginia (Charlottesville, VA).

Artificial decidual response assay and hormone treatments

Elicitation of an artificial decidual response has been described [28, 30]. Briefly, mice were ovariectomized at 6 weeks of age and rested for 2 weeks before receiving three daily subcutaneous (sc) injections of E2 (100 ng). Following 2 days of rest, mice were administered three daily sc injections of E2 plus P4 (E2 (6.7 ng) and P4 (1 mg)). Six hours following the third E2P4 injection, sesame oil (50 μl) was instilled into the lumen of the left uterine horn (stimulated); the right horn did not receive oil (unstimulated). After intraluminal instillation of the deciduogenic stimulus, mice received daily sc injections of E2P4 for 5 days, and then weighed before euthanasia. Trimmed of mesometrial membrane and vasculature, extracted stimulated and unstimulated uterine horns from each mouse were weighed for wet-weight measurements before further analysis.

To assay the ability of P4 to suppress E2 induced uterine epithelial proliferation in the ovariectomized mouse, an established protocol with modifications was used [28]. Briefly, mice were ovariectomized at 6 weeks of age, rested for 2 weeks before injection with (1) 100 μl of hormone vehicle (sesame oil; termed untreated); (2) E2 (100 ng/100 μl) for 18 h; or (3) E2 (100 ng/100 μl) and P4 (1 mg/100 μl) for 24 h before euthanasia. Tissues were immediately removed for histological examination.

Immunohistochemical analyses

Tissues, fixed in 4% PFA overnight, were processed and embedded in paraffin as previously reported [28]. Tissue sections from serially sectioned tissue blocks were placed on Superfrost plus glass slides (Fisher Scientific, Pittsburgh, PA). Prior to immunohistochemical analysis, sections were deparaffinized, rehydrated, and processed through an antigen unmasking step. Following a 1-h blocking step at room temperature, tissue sections were incubated with one of the appropriate antibodies listed in Supplementary Table S1 overnight at 4°C. After primary antibody incubation, sections were incubated with a goat anti-rabbit IgG secondary antibody (Vector laboratories Inc.) for 1 h at room temperature followed by incubation with the R.T.U Vectastain® Universal ABC reagent (Vector laboratories Inc.) for 30 min at room temperature. Immunopositivity was visualized in situ through incubation with 3, 3′-diaminobenzidine (DAB, Vector laboratories Inc.); slides were counterstained with hematoxylin for contrast. Finally, sections were dehydrated before coverslips were mounted using slowfade mounting medium (Fisher Scientific Inc.). For 5′-bromo-2′-deoxyuridine (BrdU) immunohistochemical analysis, mice were first IP injected with BrdU (10 mg/ml; Amersham Biosciences Corporation, Piscataway, NJ (0.1 ml/10 g body weight)) 2 h before euthanasia. Following tissue processing as described above, tissue sections were incubated with a biotinylated anti-BrdU antibody (BrdU In-Situ Detection Kit (BD Pharmingen Inc., San Jose, CA; 1:10 dilution)) overnight at room temperature. Sections were then incubated with the Vectastain ABC reagent at room temperature for 1 h and the immunoreaction was visualized using the DAB peroxidase substrate kit and subsequently processed as described above.

Raw images of immunostained tissue sections were digitally captured using a color chilled AxioCam MRc5 digital camera interfaced with a Carl Zeiss AxioImager A1 upright microscope (Zeiss, Jena, Germany). Postprocessing, collation, and annotation of images were performed with Photoshop and Illustrator (version 6) software programs (Adobe Systems Inc., San Jose, CA).

Molecular analyses

For studies using quantitative real-time PCR, total RNA was extracted from homogenized tissues using TRIzol® reagent (ThermoFischer Scientific Inc., Waltham, MA) and further purified using the RNeasy® Plus Mini Kit (Qiagen). Reverse transcription of total RNA into cDNA was performed using the Superscript IV VILO Master Mix (ThermoFisher Scientific Inc.) before real-time PCR amplification. Details on TaqMan ® gene expression assays used in these studies are provided in Supplementary Table S2; the 18S ribosomal RNA TaqMan® assay was used as an internal control. To evaluate *Spop* transcript levels by real-time PCR, the SensiFAST SYBR® Hi-ROX One-Step kit (Bioline Inc., #BIO-82005) was used. The sequences of the PCR primers in the 5′-3′reaction are as follows: *Spop* forward primer: GGAGGAAATGGGTGAAGTCAT; *Spop* reverse primer: GGGTTTACTCGCAAACACCA; *β-actin* forward primer: GTGGTACGACCAGAGGCATAC; and *β-actin* reverse primer: AAGGCCAACCGTGAAAAGAT.

Conditions for western immunoblotting have been described previously [31]; the primary antibodies used in these studies are listed in Supplementary Table S1. The SuperSignal West Pico Chemiluminescent Substrate kit (ThermoFisher Scientific) was used to detect the chemiluminescent signal. To facilitate the re-probing of western blots with different antibodies when required, immunoblots were stripped of primary and secondary antibodies using Restore Western Blot Stripping buffer ((#21059) Thermo Fisher Scientific Inc.).

Statistical analyses

When applicable, two-tailed Student *t* tests along with one-way ANOVA with Tukey post hoc multiple range tests were performed using the GraphPad Prism and Instat tools (GraphPad Software Inc., La Jolla, CA). A *P*-value < 0.05 was considered statistically significant; asterisks in figures denote the level of significance: $^{*}P < 0.05$; $^{**}P < 0.01$; and $^{***}P < 0.001$.

Results

The *Spop*$^{d/d}$ female mouse is infertile

Because whole body abrogation of SPOP expression in the mouse results in early neonatal death [1, 13, 25], we used a recently engineered mouse (the *Spop*$^{f/f}$ mouse) in which critical exons (encoding the MATH domain [7]) of the *Spop* gene are flanked (or floxed) by loxP sites to allow for tissue selective ablation of SPOP with a cre driver of choice (Figure 1A and B). The *Spop*$^{f/f}$ mouse was recently used by our colleague, Dr Nicholas Mitsiades at Baylor College of Medicine, to successfully abrogate SPOP in the prostate epithelium using the *probasin-cre* driver mouse [13]. Crossing the *Spop*$^{f/f}$ mouse with our *Pgr-cre* mouse [27] to generate the *Spop*$^{d/d}$ bigenic (Figure 1A and B), we similarly demonstrated that uterine *Spop* transcript levels are significantly reduced in the *Spop*$^{d/d}$ uterus (Figure 1C); importantly, western analysis did not detect SPOP protein in the *Spop*$^{d/d}$ uterus (Figure 1D). Unfortunately, we and others [13] have not been able to find a commercial SPOP antibody suitable for immunohistochemistry on adult murine tissues. Irrespective, numerous studies have shown that the *Pgr-cre* driver can successfully ablate gene expression in PGR-positive cells of the murine uterus (reviewed in [32]).

Long-term breeding studies revealed that *Spop*$^{d/d}$ female mice mated with stud males exhibited a comparable vaginal plugging latency to control females. Unlike control females (N = 12; 60 litters; 395 pups; average number of pups per litter = 6.58); however, none

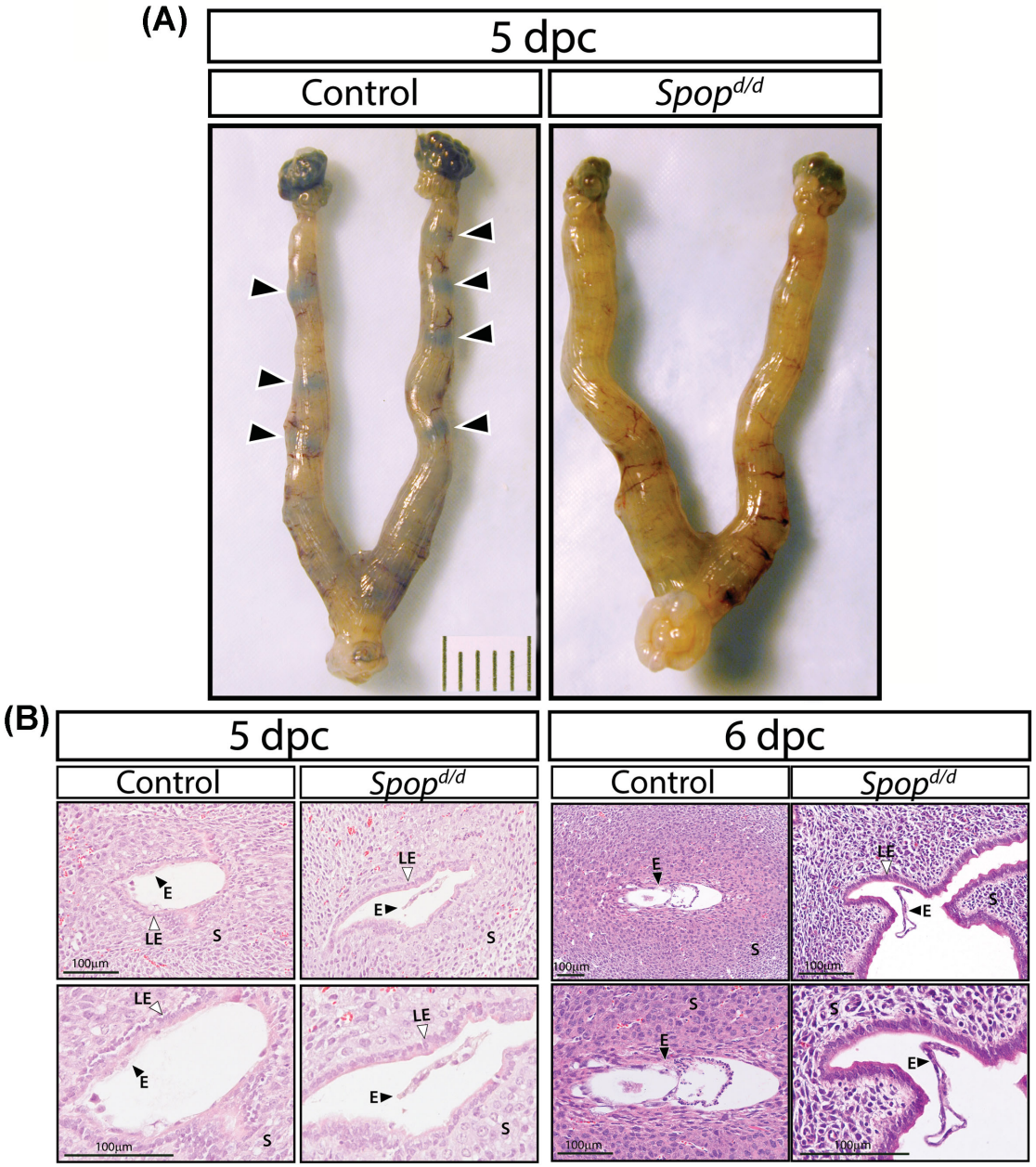

Figure 2. Embryo attachment and implantation fails in *Spop*$^{d/d}$ mice. (A) At the gross level, the location of implantation sites are clearly observed as blue bands (indicated by arrowheads) in uteri of control 5 dpc mice (n = 5) following tail vein injection with 1% Chicago sky blue dye. However, blue bands are not observed in the uterus of similarly treated *Spop*$^{d/d}$ mice (n = 6). (B) Serial sections stained with hematoxylin and eosin (H&E) of uterine tissue from control and *Spop*$^{d/d}$ mice at 5 dpc clearly show tight embryo attachment (E; black arrowhead) to the intact luminal epithelium (LE; white arrowhead) of the control mouse (n = 5); however, embryo attachment does not occur in *Spop*$^{d/d}$ mice (n = 6). Similarly, continued advancement of embryo implantation following breakdown of the luminal epithelium is seen in control 6 dpc mice (n = 5) but not in *Spop*$^{d/d}$ 6 dpc mice (n = 5); instead, the latter show floating embryos in the uterine lumen. Note: bottom panels are high power magnifications of images shown in the upper panels.

of the plugged *Spop*$^{d/d}$ females (N = 11) became pregnant over the 6-month breeding period. To examine whether impairment of ovarian function underpinned the *Spop*$^{d/d}$ infertility phenotype, prepubescent *Spop*$^{d/d}$ and control females were superovulated by administrating an established gonadotropin hormone sequential treatment regimen [28]. Both oocyte counts and ovarian histological evaluation clearly showed that ovarian activity in the *Spop*$^{d/d}$ female is comparable to that of control females (Supplementary Figure S1). This observation is further supported by the finding that *Spop*$^{d/d}$ females display a normal iterative estrous cycle profile by cytological evaluation of vaginal lavages taken daily (Supplementary Figure S1).

Because ovarian activity in the *Spop*$^{d/d}$ mouse is normal, we next tested whether *Spop*$^{d/d}$ uterine function is compromised during the implantation period. Timed pregnancy studies revealed that Chicago sky blue tail vein injection did not detect nascent implantation sites in the uterine horns of the 5-dpc *Spop*$^{d/d}$ mouse as compared with similarly treated timed-pregnant controls (Figure 2A). Examination of serial H&E stained uterine sections showed typical tight embryo

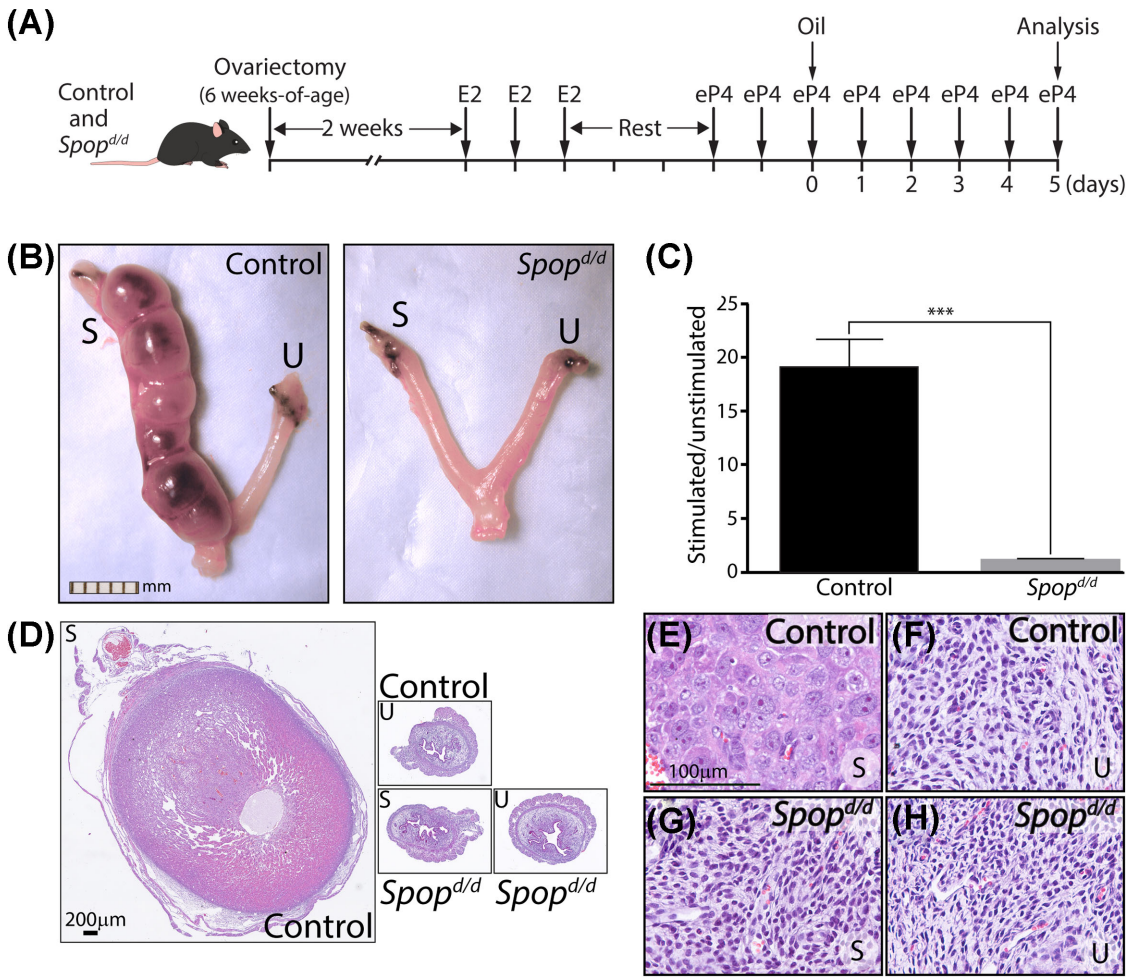

Figure 3. Uterine decidualization is impaired in the *Spop*$^{d/d}$ mouse. (A) Established protocol to induce an artificial decidual response in the uterus of ovariectomized control and *Spop*$^{d/d}$ mice (n = 6 per genotype). (B) Gross morphology of control and *Spop*$^{d/d}$ uterus following the protocol described in (A) above; stimulated and unstimulated horns are denoted by "S" and "U", respectively (scale bar applies to both panels). (C) Histogram shows the average of wet-weight ratios (±standard deviation) of stimulated uterine horns over contralateral unstimulated horns for control and *Spop*$^{d/d}$ mice; $^{***}P$-value $\leq$ 0.001. (D) Low power magnification images of H&E stained transverse sections of stimulated (S) control uterine horn; unstimulated (U) control horn; stimulated (S) *Spop*$^{d/d}$ horn; and unstimulated *Spop*$^{d/d}$ horn. Panels (E–H) are corresponding higher magnification images of regions within images shown in (D); scale bar in (E) also applies to (F–H).

attachment to the luminal epithelial compartment of the 5-dpc control uterus; however, embryo attachment was not observed in the 5-dpc or 6-dpc *Spop*$^{d/d}$ uterus (Figure 2B). In all cases, embryos were found floating in the luminal space of the *Spop*$^{d/d}$ uterus with no evidence of local luminal cavity closure around the embryo (Figure 2B). At 5 dpc, there was no significant difference in the serum levels of P4 and E2 in *Spop*$^{d/d}$ and control mice (P4 levels (ng/ml): *Spop*$^{d/d}$ = 25.0 ± 2.5; control = 22.9 ± 2.0; and E2 levels (pg/ml): *Spop*$^{d/d}$ = 4.0 ± 0.6; control = 3.6 ± 0.6; n = 6 mice per group)). These results show that ovarian luteal function is normal in the *Spop*$^{d/d}$ mouse during this period and concur with ovarian data presented in Supplementary Figure S1.

The *Spop*$^{d/d}$ infertility phenotype is intrinsic to the uterus

To confirm that the *Spop*$^{d/d}$ female infertility phenotype originates in the uterus, we used a standard artificial decidual response assay [30] on steroid hormone treated ovariectomized *Spop*$^{d/d}$ and control siblings (Figure 3). Using an E2 and P4 administration regimen shown in Figure 3A, we found that the *Spop*$^{d/d}$ uterine horn does not develop into a typical deciduoma following intraluminal instillation of sesame oil, which was the deciduogenic stimulus used in these experiments (Figure 3B–H). This result strongly supports a critical role for SPOP in steroid hormone-dependent endometrial stromal decidualization, a cellular process that is essential for the early establishment of pregnancy.

The expression level of PGR is markedly reduced in the murine *Spop*$^{d/d}$ uterus

Of the key uterine molecular signaling cues examined by western analysis, our first line of molecular investigations revealed that the expression level of both isoforms of PGR protein is markedly decreased in *Spop*$^{d/d}$ uteri as compared to control uteri of virgin mice (Figure 4A). This finding was unexpected as one study using cultured

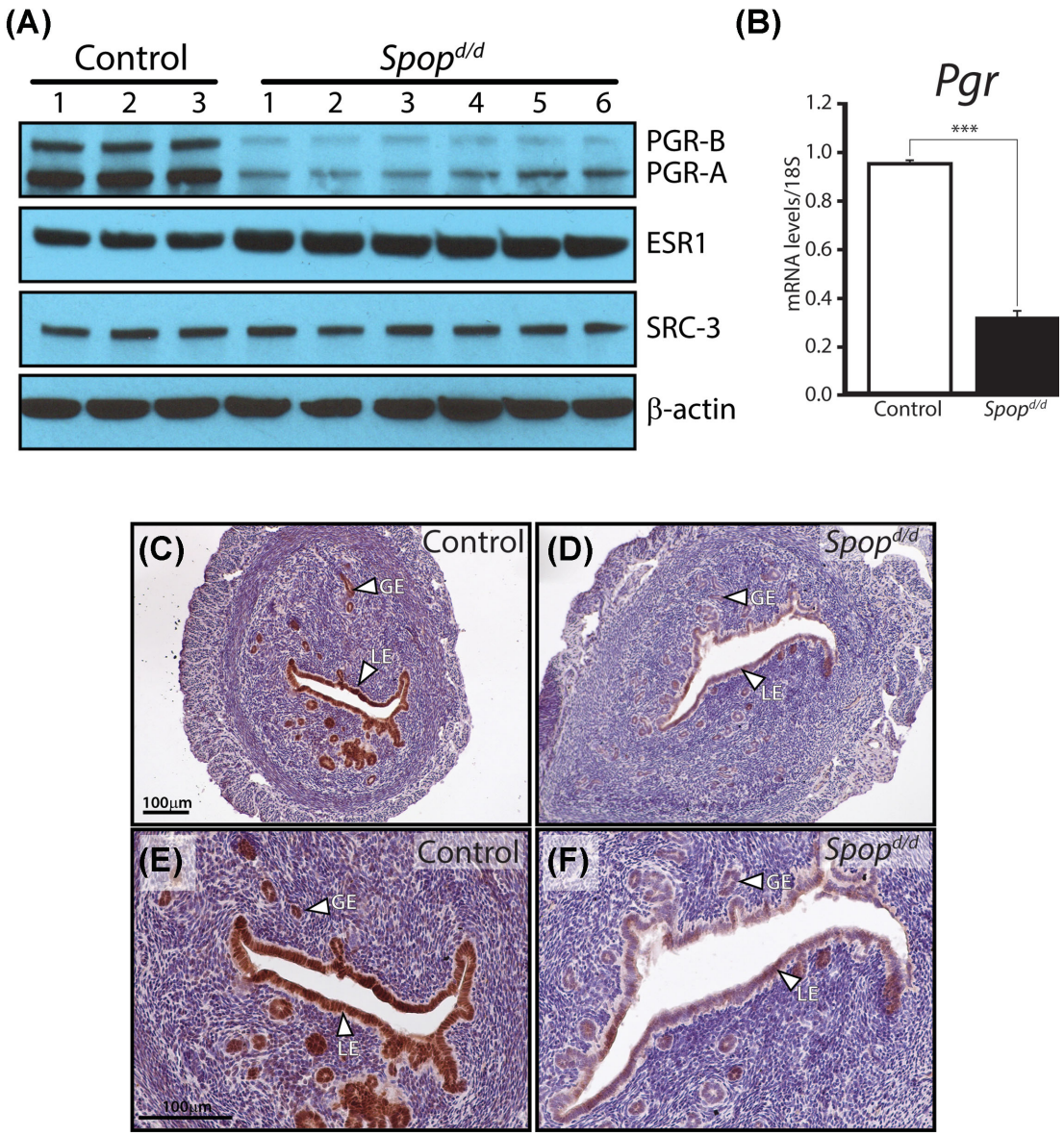

Figure 4. Protein levels of the PGR are significantly reduced in the *Spop*$^{d/d}$ uterus. (A) Western immunoblot analysis shows that the A and B isoforms of PGR are significantly reduced in the *Spop*$^{d/d}$ uterus as compared to controls. Expression levels of ESR1 are moderately increased in the *Spop*$^{d/d}$ uterus compared to controls. The expression levels for SRC-3 are not significantly changed between control and *Spop*$^{d/d}$ uteri; β-actin serves as the loading control. Note: each lane on the gel represents pooled protein samples from three individual mice. (B) Real-time PCR analysis shows that *Pgr* transcript levels are also significantly reduced in the *Spop*$^{d/d}$ uterus (n = 4) as compared to controls (n = 4). (C) Immunohistochemical detection of PGR expression in the uterus of an ovariectomized control mouse. Note strong immunoreactivity for PGR in the luminal epithelium (LE) and glandular epithelium (GE). (D) Immunohistochemical detection of PGR expression in the uterus of an ovariectomized *Spop*$^{d/d}$ mouse; note the significantly low levels of PGR expression in the luminal and glandular epithelial compartments. (E) and (F) are higher magnification images of (C) and (D) respectively; scale bar in (C) and (E) applies to (B) and (F), respectively.

human breast cancer cells showed that PGR protein is targeted for turnover by SPOP [33], suggesting absence of SPOP would lead to an increase (rather than a decrease) in the levels of uterine PGR. However, real-time PCR analysis demonstrated that *Pgr* transcript levels are also reduced by SPOP silencing (Figure 4B), indicating that the observed reduction in uterine PGR expression levels is most likely an indirect molecular consequence of SPOP depletion.

Although the expression levels of ESR1 are moderately increased in the *Spop*$^{d/d}$ uterus (Figure 4A), the induction of established ESR1 molecular targets is not significantly different between the *Spop*$^{d/d}$ and control uterus (Supplementary Figure S2). The expression levels of steroid receptor coactivator 3 (SRC-3) are unchanged between genotypes (Figure 4A). Apart from their importance in murine uterine function [34, 35], ESR1 and SRC-3 have been shown to be targets of SPOP in vitro [8, 36] as well as substrates for other ubiquitin-mediated mechanisms of protein turnover [34]. We also detected a moderate increase in protein levels of GATA2 and SRC-2 in the *Spop*$^{d/d}$ uterus as compared to the control uterus (Supplementary Figure S3); importantly, these proteins exert important roles in endometrial responsiveness to P4 [29, 37, 38].

The significant depletion of uterine PGR in the *Spop*$^{d/d}$ mouse was also confirmed by follow-up immunohistochemical detection for

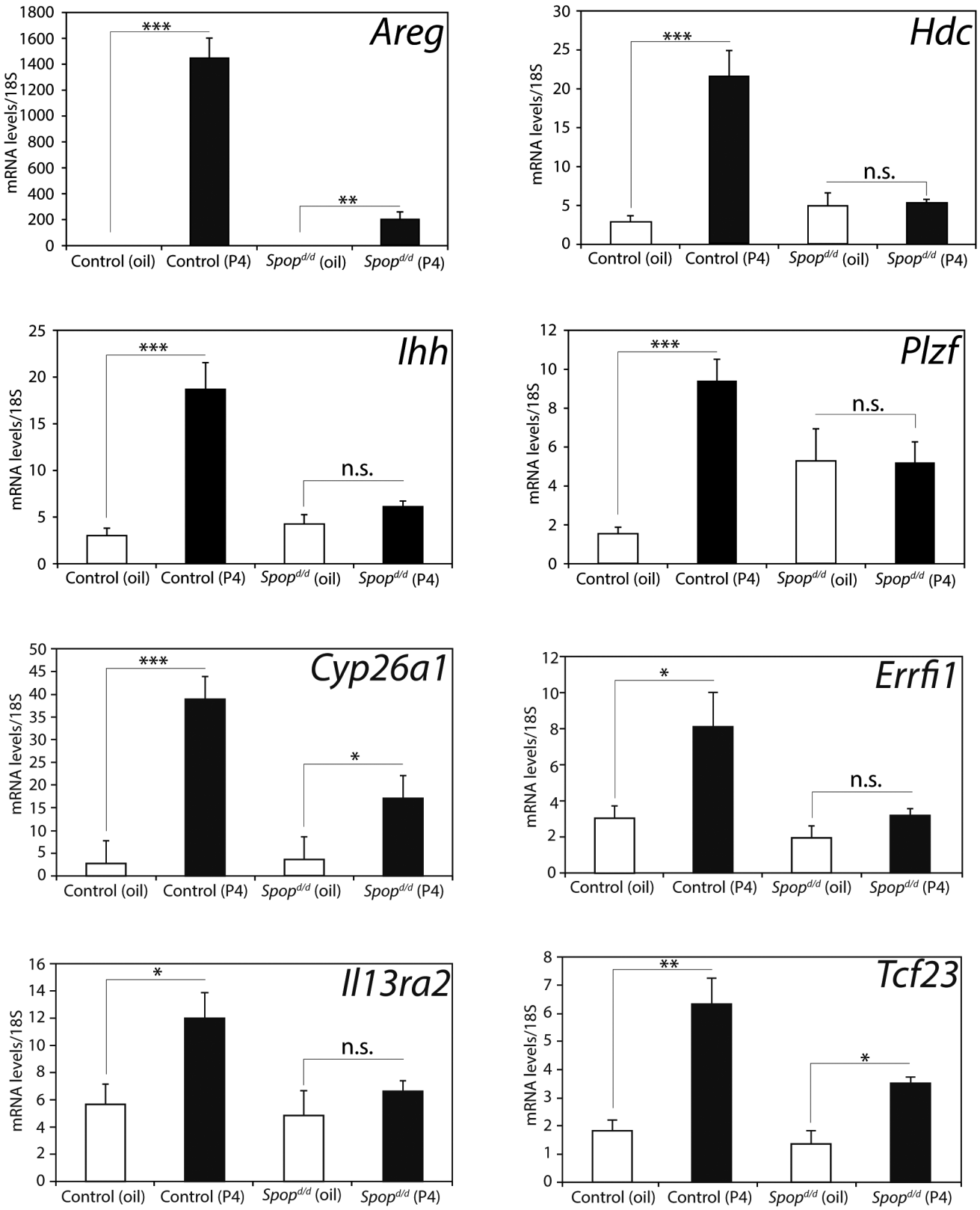

Figure 5. Absence of SPOP in the murine uterine results in a significant attenuation in the induction of established transcriptional responses to acute progesterone exposure. Quantitative real-time PCR analysis of the transcriptional induction of established P4 gene targets in the uterus from ovariectomized control and *Spop*$^{d/d}$ mice treated with vehicle (sesame oil (white column)) and 1 mg P4 (1 mg/100 μl (black column)) for 6 h (n = 5 mice per treatment/genotype). Note the marked decrease in transcriptional induction of *Areg*; *Hdc*; *Ihh*; *Plzf*; *Cyp26a1*; *Errfi1*; *IL13ra2*; and *Tcf23* in the *Spop*$^{d/d}$ uterus in response to P4 administration. *P* values $\leq$0.05, $\leq$0.01 and $\leq$0.001 are indicated by *, **, and *** respectively; n.s. denotes nonspecific ($P > 0.05$).

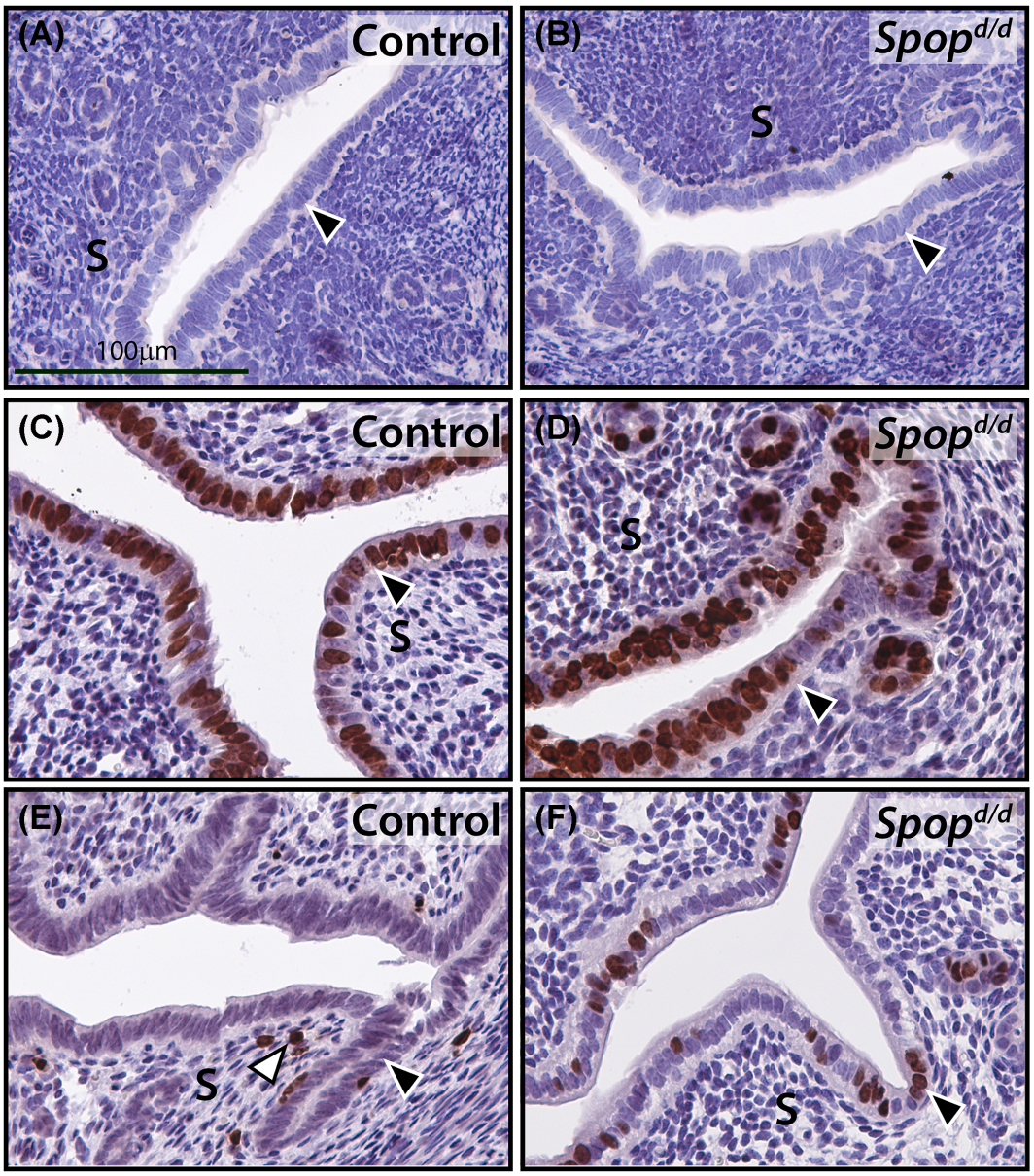

Figure 6. Progesterone suppression of estrogen-induced epithelial proliferation is significantly attenuated in the *Spop*$^{d/d}$ endometrium. (A) Uterine tissue from ovariectomized untreated control mice that were stained for BrdU incorporation. Luminal epithelium is indicated by arrowhead. (B) Uterine tissue from ovariectomized untreated *Spop*$^{d/d}$ mice that were similarly stained for BrdU incorporation. (C) Uterine tissue from ovariectomized control mice treated with E2 (100 ng for 18 h) that were stained for BrdU incorporation. Note the expected increase in the number of luminal epithelial cells that score positive for BrdU incorporation (arrowhead). (D) Uterine tissue from ovariectomized *Spop*$^{d/d}$ mice treated with E2 (100 ng for 18 h) that were stained for BrdU incorporation. Note a similar increase in the number of luminal epithelial cells scoring positive for BrdU incorporation. (E) Uterine tissue from ovariectomized control mice treated with E2 for 18 h and then P4 (1 mg) for 8 h that were stained for BrdU incorporation. Note the expected marked reduction in the number of luminal epithelial cells scoring positive for BrdU incorporation (black arrowhead). White arrowhead indicates a stromal cell positive for BrdU incorporation. (F) Uterine tissue from ovariectomized *Spop*$^{d/d}$ mice treated with E2 for 18 h and then P4 (1 mg) for 8 h that were stained for BrdU incorporation. Note: a significant number of luminal epithelial cells remain positive for BrdU incorporation (arrowhead). Scale bar in (A) applies to (B–F); data representative of n = 5 mice per genotype/treatment group.

PGR expression in uterine sections derived from untreated ovariectomized *Spop*$^{d/d}$ and control mice (Figure 4C–F). It is known that PGR protein expression is markedly robust and consistent in the epithelial compartment of the uterus of the ovariectomized wild-type mouse [38], making for an ideal model to compare the relative expression levels of this nuclear receptor in control and mutant mice by immunohistochemistry [38]. Importantly, as a consequence of the reduction of uterine PGR levels, the transcriptional induction of a number of PGR molecular targets is significantly attenuated in the *Spop*$^{d/d}$ uterus (Figure 5), a subset of these targets are critical for embryo implantation [39–41] and endometrial stromal cell decidualization [31, 42].

Reduction in PGR levels in the *Spop*$^{d/d}$ uterus also results in a significant attenuation in the ability of P4 to suppress E2-induced uterine epithelial proliferation (Figure 6). This result is significant as endometrial P4 resistance is linked to a number of

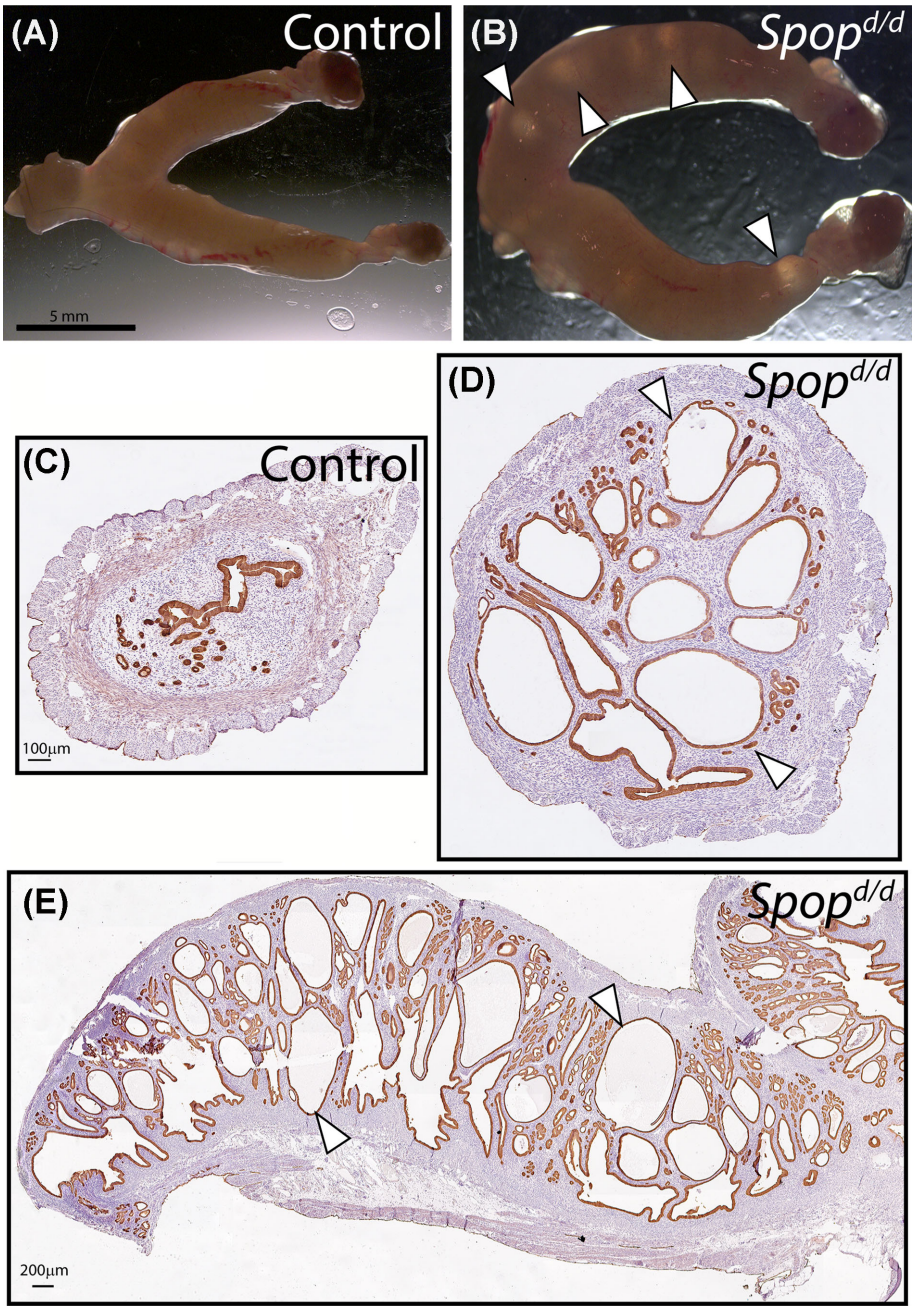

Figure 7. The *Spop*$^{d/d}$ uterus exhibits large cystic endometrial glands with age. (A) Light microscopy using a dissecting scope of control uterine tissue at the gross level (n = 5 mice). (B) Light microscopy of *Spop*$^{d/d}$ uterus shows conspicuously large cysts (arrowheads); n = 5 mice. Scale bar in (A) applies to (B). (C) Transverse section of control uterus stained for cytokeratin 8, an epithelial marker. (D) Transverse section of *Spop*$^{d/d}$ uterus similarly stained for cytokeratin 8; note the numerous large glandular epithelial cystic structures (arrowhead). Scale bar in (C) applies to (D). (E) Longitudinal section of the *Spop*$^{d/d}$ uterus stained for cytokeratin 8. Note that cystic glands of variable size and shape appear throughout the uterine horn (arrowhead).

endometrial pathologies, including endometriosis and endometrial cancer [43].

Cystic endometrial glands develop in the *Spop*$^{d/d}$ uterus with age

By 10 months of age, the untreated *Spop*$^{d/d}$ uterus exhibits overt dilated cystic glandular structures that are not observed in age-matched control mice (Figure 7A–E). Throughout the *Spop*$^{d/d}$ uterine horn, numerous cystoid structures—irregular in size and shape—crowd the endometrial stroma in cribriform patterns that extend to the circular smooth muscle layer of the myometrium (Figure 7A–E). However, the dilated *Spop*$^{d/d}$ uterine glands do not show epithelial atypia, pseudostratification, or excessive secretory (or eosin positive) material. Interestingly, immunohistochemical evaluation for FOXA2 expression (a marker for normal glandular epithelial cells [44]) is significantly reduced in epithelial cells that comprise the larger cysts, which suggests that these cells have lost their normal glandular

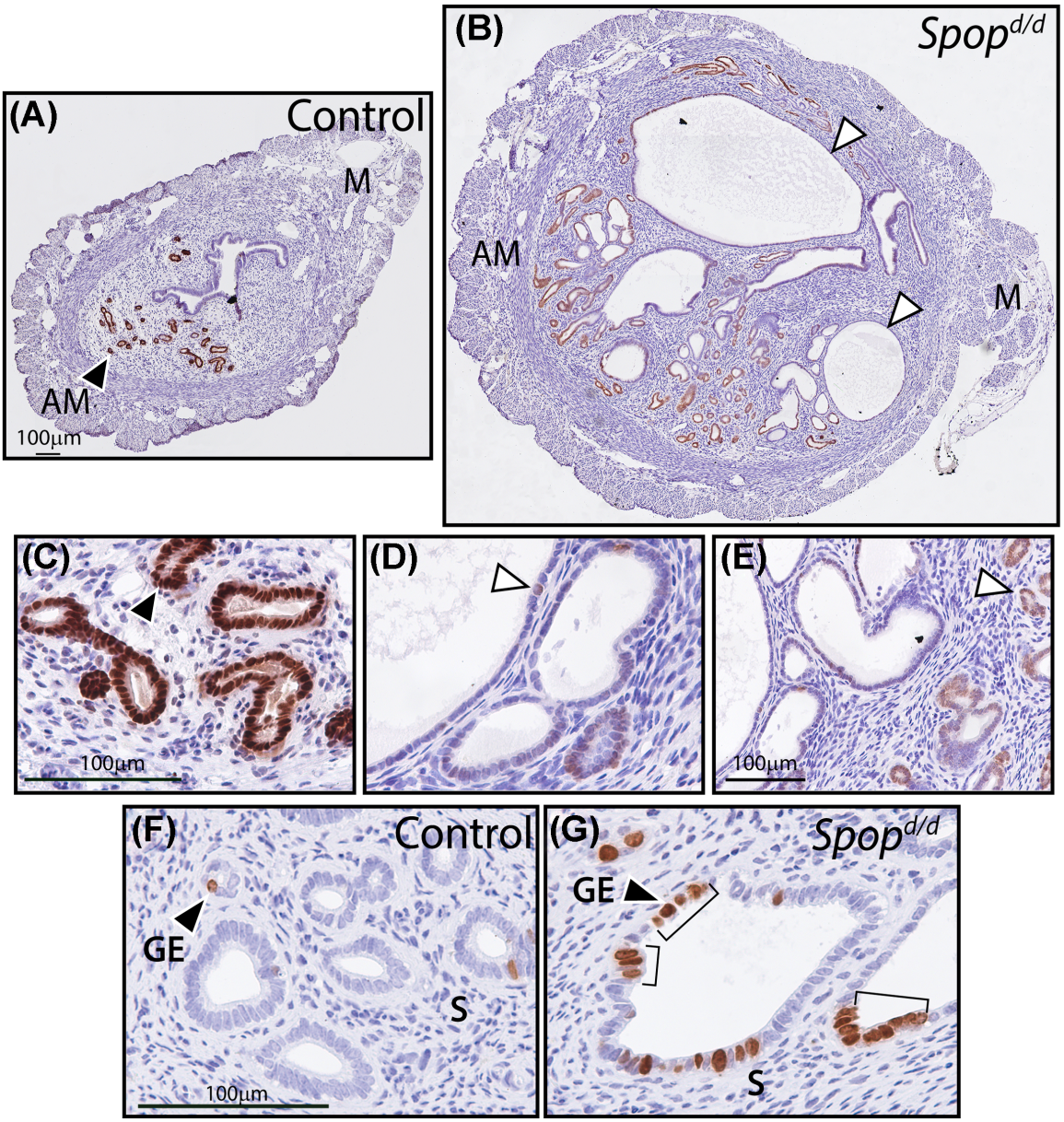

Figure 8. Epithelial cells in *Spop*$^{d/d}$ endometrial cysts express low levels of FOXA2 and exhibit increased proliferative capacity. (A) Transverse section of uterine horn from a control mouse stained for FOXA2 expression. Note the expected strong immunopositivity for FOXA2 expression in the glandular epithelia located in the antimesometrial (AM) pole (arrowhead); M indicates mesometrial pole. (B) Transverse section of uterine horn from *Spop*$^{d/d}$ mouse similarly stained for FOXA2 expression. Note the significant decreased expression of FOXA2 in the larger cystoid structures (arrowheads). Scale bar in (A) applies to (B). (C) Higher magnification of region shown in (A) above. (D) and (E) are higher magnifications of regions shown in (B) above. Scale bar in (C) applies to (D). (F) Control glandular epithelia (GE) stained for BrdU incorporation. Note the sparse distribution of BrdU-positive GE cells (arrowhead). (G) Immunostaining for BrdU incorporation in *Spop*$^{d/d}$ GE cells. Note the foci (brackets) of BrdU-positive cells in the larger cystic glands; S indicates stroma. Scale bar in (F) applies to (G).

epithelial identity (Figure 8A–E). Although the *Spop*$^{d/d}$ glandular epithelium scores significantly higher in the number of proliferating cells as compared to controls, many of these proliferating cells are distributed in focal areas rather than evenly distributed (Figure 8F and G); this cellular distribution pattern has been reported for similar uterine pathologies with dilated cystic uterine glands [45]. Therefore, the *Spop*$^{d/d}$ uterine histopathology that emerges with age may arise from these foci of hyperproliferation.

Discussion

Although SPOP was discovered over two decades ago [46], conditional SPOP knockout mouse models have only been generated and characterized within the last two years [13, 25]. In the case of the murine prostate, SPOP ablation in the epithelium results in hyperplasia and dysplasia that develops into prostatic intraepithelial neoplasia (PIN) in the dorsolateral and ventral prostate by 38 weeks of age [13]. Using a similar approach that allows for the targeted ablation

of SPOP in cells which express PGR, we demonstrate the importance of uterine SPOP for embryo implantation and endometrial decidualization. By revealing a critical role for SPOP in hormone-dependent endometrial decidualization, we provide essential in vivo support for recent in vitro studies [47] that report a pivotal involvement for murine SPOP in endometrial stromal cell decidualization in culture.

Intriguingly, our molecular analysis demonstrates that the expression levels of both isoforms of the PGR protein are significantly attenuated with uterine SPOP depletion, providing one mechanistic explanation for the uterine dysfunction displayed by the $Spop^{d/d}$ mice. The marked reduction in PGR protein levels following SPOP ablation was unexpected since SPOP has been shown by in vitro studies to turnover PGR [33] as well as other nuclear receptors, such as ESR1 and the AR [9, 36, 48, 49]. Moreover, a recent in vivo study—using a similar engineered mouse approach—showed that the expression levels of AR—a close relative of PGR—are markedly increased as expected in the prostate epithelium following conditional SPOP ablation in the mouse [13]. However, the observation that *Pgr* transcript levels are also reduced in the $Spop^{d/d}$ uterus argues for an indirect regulation of PGR protein levels by SPOP. Instead, these findings suggest other regulatory factors of PGR protein stability and/or transcription are substrates for uterine SPOP. Accordingly, the striking reduction in uterine PGR expression levels results in adverse molecular repercussions in terms of a significant attenuated induction of key downstream transcriptional programs required for endometrial implantation processes and decidualization in the mouse. Furthermore, the P4 resistance phenotype of the $Spop^{d/d}$ uterus may suggest a cellular mechanism to explain the functional defects of this tissue, when SPOP function is derailed. The latter proposal will be a major focus for future investigations.

Further molecular analysis disclosed that SPOP ablation results in a moderate increase in the expression levels of uterine ESR1, GATA2, and SRC-2, suggesting that perturbation of SPOP action most likely derails the normal homeostatic levels of many proteins in the proteome required for uterine function. Although the changes in expression levels are moderate for a given protein, we speculate that the collective alterations in levels of many proteins are expected to exert significant adverse effects on uterine function. Interestingly, we have recently shown that GATA2 is required for maintaining uterine PGR expression levels [38]. The observation that GATA2 is moderately increased in the $Spop^{d/d}$ uterus may represent a molecular mechanism to increase PGR expression in response to the significant decrease in PGR expression levels as result of SPOP ablation. In the case of SRC-2, we previously demonstrated that increasing the levels of this coregulator results in severe uterine dysfunction in the mouse [29], resulting in a striking subfertility phenotype. The uterine defects resulting from increased SRC-2 levels include a marked impairment in uterine decidualization and an enhanced proliferative response to E2 exposure leading to endometrial glandular cysts and epithelial hyperplasia [29].

In view of the strengthening link between *SPOP* somatic mutations and a subset of human endometrial cancers [2–5], the question arose as to whether the $Spop^{d/d}$ uterus would exhibit histopathological signatures consistent with the early stages of endometrial tumorigenesis. Although the $Spop^{d/d}$ conditional knockout allele in the mouse does not directly model the human *SPOP* point mutations found in human endometrial cancers, both *SPOP* mutation types result in loss-of-function phenotypes. In keeping with recent in vivo prostate studies in the mouse [13], we found that the aging $Spop^{d/d}$ endometrium develops conspicuously dilated glandular epithelial cysts with foci of hyperproliferative epithelial cells. Interestingly, these aberrant histomorphic features emerge at approximately the same time (~38–40 weeks) that PIN lesions are observed in the prostate of mice in which the *Spop* allele is conditionally abrogated [13]. Whether the histopathology of the $Spop^{d/d}$ endometrium predisposes this tissue to neoplasia with time or accelerates the progression of oncogene-dependent endometrial cancer constitute important questions for future investigation.

Supplementary data

Supplementary data are available at *BIOLRE* online.

Supplementary Table S1. List of antibodies used in the describe experiments.
Supplementary Table S2. List of TaqMan assays used in the described experiments.
Supplementary Figure S1. Ovarian function is normal in the $Spop^{d/d}$ mouse. (A) Control (n = 8) and $Spop^{d/d}$ (n = 6) mice ovulated similar numbers of oocytes following administration of an established superovulation hormone regimen. (B–E) Histological analysis shows both control (B, D) and $Spop^{d/d}$ (C, E) ovaries exhibit corpora lutea (CL) following ovulation. (F) Typical estrous cyclicity profiles for both control (n = 10) and $Spop^{d/d}$ (n = 10) mice supports normal ovarian activity including steroidogenesis in $Spop^{d/d}$ female. (G) Representative examples of crystal violet stained vaginal cytology from control and $Spop^{d/d}$ mice at defined stages of the estrous cycle.
Supplementary Figure S2. Expression of estrogen molecular targets is not significantly altered in the $Spop^{d/d}$ uterus.
Supplementary Figure S3. Western analysis of GATA2, SRC-1, and SRC-2 protein expression in the control and $Spop^{d/d}$ uterus.

Acknowledgments

The authors thank Jie Li, Yan Ying, and Rong Zhao for their essential technical contributions. We would also like to thank Dr Nicholas Mitsiades, Baylor College of Medicine, for providing his findings from studies on the conditional knockout of Spop in the murine prostate prior to publication. We also acknowledge the services of The University of Virginia Center for Research in Reproduction Ligand Assay and Analysis Core, supported by the Eunice Kennedy Shriver NICHD/NIH (NCTRI) grant source: P50-HD28934.

References

1. Claiborn KC, Sachdeva MM, Cannon CE, Groff DN, Singer JD, Stoffers DA. Pcif1 modulates Pdx1 protein stability and pancreatic beta cell function and survival in mice. *J Clin Invest* 2010; **120**(10):3713–3721.
2. DeLair DF, Burke KA, Selenica P, Lim RS, Scott SN, Middha S, Mohanty AS, Cheng DT, Berger MF, Soslow RA, Weigelt B. The genetic landscape of endometrial clear cell carcinomas. *J Pathol* 2017; **243**(2):230–241.
3. Jones S, Stransky N, McCord CL, Cerami E, Lagowski J, Kelly D, Angiuoli SV, Sausen M, Kann L, Shukla M, Makar R, Wood LD et al. Genomic analyses of gynaecologic carcinosarcomas reveal frequent mutations in chromatin remodelling genes. *Nat Commun* 2014; **5**:5006.
4. Le Gallo M, Bell DW. The emerging genomic landscape of endometrial cancer. *Clin Chem* 2014; **60**:98–110.
5. Program NIHISCCSLe Gallo M, O'Hara AJ, Rudd ML, Urick ME, Hansen NF, O'Neil NJ, Price JC, Zhang S, England BM, Godwin AK, Sgroi DC et al. Exome sequencing of serous endometrial tumors identifies recurrent somatic mutations in chromatin-remodeling and ubiquitin ligase complex genes. *Nat Genet* 2012; **44**:1310–1315.
6. Chen HY, Chen RH. Cullin 3 ubiquitin ligases in cancer biology: functions and therapeutic implications. *Front Oncol* 2016; **6**:113.

7. Mani RS. The emerging role of speckle-type POZ protein (SPOP) in cancer development. *Drug Discov Today* 2014; **19**:1498–1502.
8. Geng C, He B, Xu L, Barbieri CE, Eedunuri VK, Chew SA, Zimmermann M, Bond R, Shou J, Li C, Blattner M, Lonard DM et al. Prostate cancer-associated mutations in speckle-type POZ protein (SPOP) regulate steroid receptor coactivator 3 protein turnover. *Proc Natl Acad Sci USA* 2013; **110**:6997–7002.
9. Geng C, Rajapakshe K, Shah SS, Shou J, Eedunuri VK, Foley C, Fiskus W, Rajendran M, Chew SA, Zimmermann M, Bond R, He B et al. Androgen receptor is the key transcriptional mediator of the tumor suppressor SPOP in prostate cancer. *Cancer Res* 2014; **74**:5631–5643.
10. An J, Ren S, Murphy SJ, Dalangood S, Chang C, Pang X, Cui Y, Wang L, Pan Y, Zhang X, Zhu Y, Wang C et al. Truncated ERG oncoproteins from TMPRSS2-ERG fusions are resistant to SPOP-mediated proteasome degradation. *Mol Cell* 2015; **59**:904–916.
11. An J, Wang C, Deng Y, Yu L, Huang H. Destruction of full-length androgen receptor by wild-type SPOP, but not prostate-cancer-associated mutants. *Cell Rep* 2014; **6**:657–669.
12. Gan W, Dai X, Lunardi A, Li Z, Inuzuka H, Liu P, Varmeh S, Zhang J, Cheng L, Sun Y, Asara JM, Beck AH et al. SPOP promotes ubiquitination and degradation of the erg oncoprotein to suppress prostate cancer progression. *Mol Cell* 2015; **59**:917–930.
13. Geng C, Kaochar S, Li M, Rajapakshe K, Fiskus W, Dong J, Foley C, Dong B, Zhang L, Kwon OJ, Shah SS, Bolaki M et al. SPOP regulates prostate epithelial cell proliferation and promotes ubiquitination and turnover of c-MYC oncoprotein. *Oncogene* 2017; **36**: 4767–4777.
14. Groner AC, Cato L, de Tribolet-Hardy J, Bernasocchi T, Janouskova H, Melchers D, Houtman R, Cato ACB, Tschopp P, Gu L, Corsinotti A, Zhong Q et al. TRIM24 is an oncogenic transcriptional activator in prostate cancer. *Cancer Cell* 2016; **29**:846–858.
15. Kwon JE, La M, Oh KH, Oh YM, Kim GR, Seol JH, Baek SH, Chiba T, Tanaka K, Bang OS, Joe CO, Chung CH. BTB domain-containing speckle-type POZ protein (SPOP) serves as an adaptor of Daxx for ubiquitination by Cul3-based ubiquitin ligase. *J Biol Chem* 2006; **281**:12664–12672.
16. Li C, Ao J, Fu J, Lee DF, Xu J, Lonard D, O'Malley BW. Tumor-suppressor role for the SPOP ubiquitin ligase in signal-dependent proteolysis of the oncogenic co-activator SRC-3/AIB1. *Oncogene* 2011; **30**:4350–4364.
17. Wu F, Dai X, Gan W, Wan L, Li M, Mitsiades N, Wei W, Ding Q, Zhang J. Prostate cancer-associated mutation in SPOP impairs its ability to target Cdc20 for poly-ubiquitination and degradation. *Cancer Lett* 2017; **385**:207–214.
18. Zhang P, Gao K, Tang Y, Jin X, An J, Yu H, Wang H, Zhang Y, Wang D, Huang H, Yu L, Wang C. Destruction of DDIT3/CHOP protein by wild-type SPOP but not prostate cancer-associated mutants. *Human Mutat* 2014; **35**:1142–1151.
19. Zhang Q, Shi Q, Chen Y, Yue T, Li S, Wang B, Jiang J. Multiple Ser/Thr-rich degrons mediate the degradation of Ci/Gli by the Cul3-HIB/SPOP E3 ubiquitin ligase. *Proc Natl Acad Sci USA* 2009; **106**:21191–21196.
20. Zhu H, Ren S, Bitler BG, Aird KM, Tu Z, Skordalakes E, Zhu Y, Yan J, Sun Y, Zhang R. SPOP E3 ubiquitin ligase adaptor promotes cellular senescence by degrading the SENP7 deSUMOylase. *Cell Rep* 2015; **13**:1183–1193.
21. Guo ZQ, Zheng T, Chen B, Luo C, Ouyang S, Gong S, Li J, Mao LL, Lian F, Yang Y, Huang Y, Li L et al. Small-molecule targeting of E3 ligase adaptor SPOP in kidney cancer. *Cancer Cell* 2016; **30**:474–484.
22. Liu X, Sun G, Sun X. RNA interference-mediated silencing of speckle-type POZ protein promotes apoptosis of renal cell cancer cells. *Onco Targets Ther* 2016; **9**:2393–2402.
23. Stone L. Kidney cancer: on target - inhibiting SPOP in ccRCC. *Nat Rev Urol* 2016; **13**:630.
24. Zhao W, Zhou J, Deng Z, Gao Y, Cheng Y. SPOP promotes tumor progression via activation of beta-catenin/TCF4 complex in clear cell renal cell carcinoma. *Int J Oncol* 2016; **49**:1001–1008.
25. Cai H, Liu A. Spop promotes skeletal development and homeostasis by positively regulating Ihh signaling. *Proc Natl Acad Sci USA* 2016; **113**:14751–14756.
26. Farley FW, Soriano P, Steffen LS, Dymecki SM. Widespread recombinase expression using FLPeR (flipper) mice. *Genesis* 2000; **28**:106–110.
27. Soyal SM, Mukherjee A, Lee KY, Li J, Li H, DeMayo FJ, Lydon JP. Cre-mediated recombination in cell lineages that express the progesterone receptor. *Genesis* 2005; **41**:58–66.
28. Lydon JP, DeMayo FJ, Funk CR, Mani SK, Hughes AR, Montgomery CA, Jr, Shyamala G, Conneely OM, O'Malley BW. Mice lacking progesterone receptor exhibit pleiotropic reproductive abnormalities. *Genes Dev* 1995; **9**:2266–2278.
29. Szwarc MM, Kommagani R, Jeong JW, Wu SP, Tsai SY, Tsai MJ, O'Malley BW, DeMayo FJ, Lydon JP. Perturbing the cellular levels of steroid receptor coactivator-2 impairs murine endometrial function. *PLoS ONE* 2014; **9**:e98664.
30. Kommagani R, Szwarc MM, Kovanci E, Gibbons WE, Putluri N, Maity S, Creighton CJ, Sreekumar A, DeMayo FJ, Lydon JP, O'Malley BW. Acceleration of the glycolytic flux by steroid receptor coactivator-2 is essential for endometrial decidualization. *PLoS Genet* 2013; **9**:e1003900.
31. Kommagani R, Szwarc MM, Vasquez YM, Peavey MC, Mazur EC, Gibbons WE, Lanz RB, DeMayo FJ, Lydon JP. The promyelocytic leukemia zinc finger transcription factor is critical for human endometrial stromal cell decidualization. *PLoS Genet* 2016; **12**: e1005937.
32. Wu SP, DeMayo FJ. Progesterone receptor signaling in uterine myometrial physiology and preterm birth. *Curr Top Dev Biol* 2017; **125**:171–190.
33. Gao K, Jin X, Tang Y, Ma J, Peng J, Yu L, Zhang P, Wang C. Tumor suppressor SPOP mediates the proteasomal degradation of progesterone receptors (PRs) in breast cancer cells. *Am J Cancer Res* 2015; **5**:3210–3220.
34. Kawagoe J, Li Q, Mussi P, Liao L, Lydon JP, DeMayo FJ, Xu J. Nuclear receptor coactivator-6 attenuates uterine estrogen sensitivity to permit embryo implantation. *Dev Cell* 2012; **23**:858–865.
35. Lubahn DB, Moyer JS, Golding TS, Couse JF, Korach KS, Smithies O. Alteration of reproductive function but not prenatal sexual development after insertional disruption of the mouse estrogen receptor gene. *Proc Natl Acad Sci USA* 1993; **90**:11162–11166.
36. Zhang P, Gao K, Jin X, Ma J, Peng J, Wumaier R, Tang Y, Zhang Y, An J, Yan Q, Dong Y, Huang H et al. Endometrial cancer-associated mutants of SPOP are defective in regulating estrogen receptor-alpha protein turnover. *Cell Death Dis* 2015; **6**:e1687.
37. Xu J, Qiu Y, DeMayo FJ, Tsai SY, Tsai MJ, O'Malley BW. Partial hormone resistance in mice with disruption of the steroid receptor coactivator-1 (SRC-1) gene. *Science* 1998; **279**:1922–1925.
38. Rubel CA, Wu SP, Lin L, Wang T, Lanz RB, Li X, Kommagani R, Franco HL, Camper SA, Tong Q, Jeong JW, Lydon JP et al. A Gata2 -dependent transcription network regulates uterine progesterone responsiveness and endometrial function. *Cell Rep* 2016; **17**:1414–1425.
39. Han BC, Xia HF, Sun J, Yang Y, Peng JP. Retinoic acid-metabolizing enzyme cytochrome P450 26a1 (cyp26a1) is essential for implantation: functional study of its role in early pregnancy. *J Cell Physiol* 2010; **223**:471–479.
40. Kim TH, Lee DK, Franco HL, Lydon JP, Jeong JW. ERBB receptor feedback inhibitor 1 regulation of estrogen receptor activity is critical for uterine implantation in mice. *Biol Reprod* 2010; **82**: 706–713.
41. Lee K, Jeong J, Kwak I, Yu CT, Lanske B, Soegiarto DW, Toftgard R, Tsai MJ, Tsai S, Lydon JP, DeMayo FJ. Indian hedgehog is a major mediator of progesterone signaling in the mouse uterus. *Nat Genet* 2006; **38**:1204–1209.
42. Kommagani R, Szwarc MM, Kovanci E, Creighton CJ, O'Malley BW, Demayo FJ, Lydon JP. A murine uterine transcriptome, responsive to steroid receptor coactivator-2, reveals transcription factor 23 as essential for decidualization of human endometrial stromal cells. *Biol Reprod* 2014; **90**:75.
43. Kim JJ, Kurita T, Bulun SE. Progesterone action in endometrial cancer, endometriosis, uterine fibroids, and breast cancer. *Endocr Rev* 2013; **34**:130–162.

44. Kelleher AM, Peng W, Pru JK, Pru CA, DeMayo FJ, Spencer TE. Forkhead box a2 (FOXA2) is essential for uterine function and fertility. *Proc Natl Acad Sci USA* 2017; **114**:E1018–E1026.
45. Gonzalez G, Mehra S, Wang Y, Akiyama H, Behringer RR. Sox9 overexpression in uterine epithelia induces endometrial gland hyperplasia. *Differentiation* 2016; **92**:204–215.
46. Nagai Y, Kojima T, Muro Y, Hachiya T, Nishizawa Y, Wakabayashi T, Hagiwara M. Identification of a novel nuclear speckle-type protein, SPOP. *FEBS Lett* 1997; **418**:23–26.
47. Liu N, Liu X, Yu Q, Chen X, Ding Y, He J, Gao R, Wang Y, Liu X. SPOP regulates endometrial stromal cell decidualization in mice. *Reprod Sci* 2016; **23**:1565–1574.
48. Lai J, Batra J. Speckle-type POZ protein mutations interrupt tumor suppressor function of speckle-type POZ protein in prostate cancer by affecting androgen receptor degradation. *Asian J Androl* 2014; **16**:659–660.
49. Byun B, Jung Y. Repression of transcriptional activity of estrogen receptor alpha by a Cullin3/SPOP ubiquitin E3 ligase complex. *Mol Cell* 2008; **25**:289–293.